# Transient Wind-driven Polynyas Within Nares Strait

**Kevin Joshy[1], G.W.K. Moore[1, 2], Kaitlin McNeil[1, 2]**

[1]Department of Chemical and Physical Sciences, University of Toronto, Mississauga, Mississauga, Canada. [2]Department of Physics, University of Toronto, Toronto, Canada.

Corresponding author: G. W. K. Moore (gwk.moore@utoronto.ca)

**Key Points:**

- Previously unknown wind-driven polynyas form downwind of Joe and Franklin Islands within Nares Strait during autumn months
- The presence of these islands interrupting the sea ice flow through the strait are proposed to be the drivers inducing polynya formation
- The size and extent of these polynyas was correlated with wind speed flowing southwards through the strait

## Abstract

Nares Strait, situated between northwest Greenland and Ellesmere Island is a major sea ice export path from the Arctic Ocean. One of the narrowest parts of the strait — Kennedy Channel — is host to several islands. These obstacles' impact on the ice flow along the Strait has yet to be investigated. Here we show that during autumn, these islands can interrupt the relatively homogenous sea ice flow through Kennedy Channel, carried by wind and water currents, and shield downstream regions from becoming ice-covered, resulting in the formation of hitherto unknown transient polynyas, whose size and extent were correlated with the wind's strength and direction along Kennedy Channel. These polynyas likely impact the regional meteorology and oceanography through enhanced air-sea fluxes of heat, moisture, momentum, and carbon dioxide. The presence of open water may also impact the complex and productive regional ecosystem.



## Plain Language Summary

Nares Strait is a passageway situated between Ellesmere Island — the northernmost island of Nunavut, Canada — and Greenland. The southern end of this channel is the site of formation of the North Water Polynya (NOW) which is an open water expanse that forms in the midst of thick surrounding ice. Open water regions of polynyas throughout the world, in general, have major impacts on local climates because they facilitate interactions from the atmosphere to the sea and vice versa. The NOW in particular sustains a major Arctic ecosystem that nearby human communities depend on for resources as well. We identify polynyas that form in the interior of Nares Strait during autumn whose sizes are related to the strength of southward winds blowing through the channel. These polynyas likely also impact the regional climate and ocean dynamics, and may serve as a site of Arctic species habitation both in the present and in a future where the integrity of the NOW is potentially compromised due to a changing Arctic environment.


## 1 Introduction

Polynyas are defined as regions of open water found within a surrounding area of sea ice and tend to form by two distinct mechanisms (Barber & Massom, 2007); those that form via the melting of ice due to heat fluxes from processes such as the upwelling of warm waters are called sensible heat polynyas (Smith et al., 1990), while those that form via the exposure of open water

by winds that drive away ice cover are referred to as latent heat or wind-driven polynyas (Barber & Massom, 2007). Despite this classification, many polynyas around the world form as a result of some combination of these two effects (Barber & Massom, 2007).

Polynyas are important meteorologically, oceanographically, and biologically. They contribute to atmospheric forcing via significant sea-air heat and moisture fluxes (Kottmeier & Engelbart, 1992), they influence ocean salinity via processes such as frazil ice formation and brine rejection (Smith et al., 1990), as well as encouraging the formation of dense water (Weingartner et al., 1998). Biologically, they allow for the upwelling and mixing of nutrient-rich waters (Arrigo, 2007) which, in combination with enhanced solar insolation at the active polynya site (Tremblay & Smith, 2007), encourage biological activity.

Nares Strait, a passageway situated between Ellesmere Island, the northernmost island of Canada, and northwestern Greenland (Fig. 1) connects the Arctic Ocean at its north to the subpolar North Atlantic at its south. Nares Strait is a significant site of sea ice export, which is driven by wind and ocean currents, out of the Arctic Ocean and experiences an average seasonal sea ice area flux on the order of $100 \times 10^3$ km$^2$ (Howell et al., 2023). This is approximately 10% of the export through Fram Strait (Smedsrud et al., 2017).

The polynya that forms annually over northern Baffin Bay — the North Water Polynya (NOW) — *Pikialasorsuaq* in Greenland (Moore et al., 2023) and *Sarvarjuaq* in Nunavut — appears as a result of the cessation of sea ice flow through the strait due to the formation of an ice arch near the strait's southern terminus (Barber et al., 2001; Ribeiro et al., 2021). The inhibition of further sea ice flow by these arches, alongside the wind-forced advection of sea ice out of the downstream region (Barber et al., 2001; Moore & Imrit, 2022), and the melting of ice via the thermodynamic interaction with warm subsurface waters (Steffen, 1985) are together suggested to maintain the integrity of the NOW (Ingram et al., 2002).

A large body of evidence suggests the presence of a vast ecosystem that the NOW sustains. Phytoplankton blooms are common and promoted in polynyas (Marchese et al., 2017; Tremblay & Smith, 2007), which act as a foundation for an Arctic food web. Several animal populations have also been documented in this region such as beluga whales, narwhals, walruses, bearded seals, seabirds, as well as limited sightings of polar bears, many of which overwinter in the NOW (Finley & Renaud, 1980; Heide-Jørgensen et al., 2013, 2016; Møller et al., 2018; Richard et al., 1998).

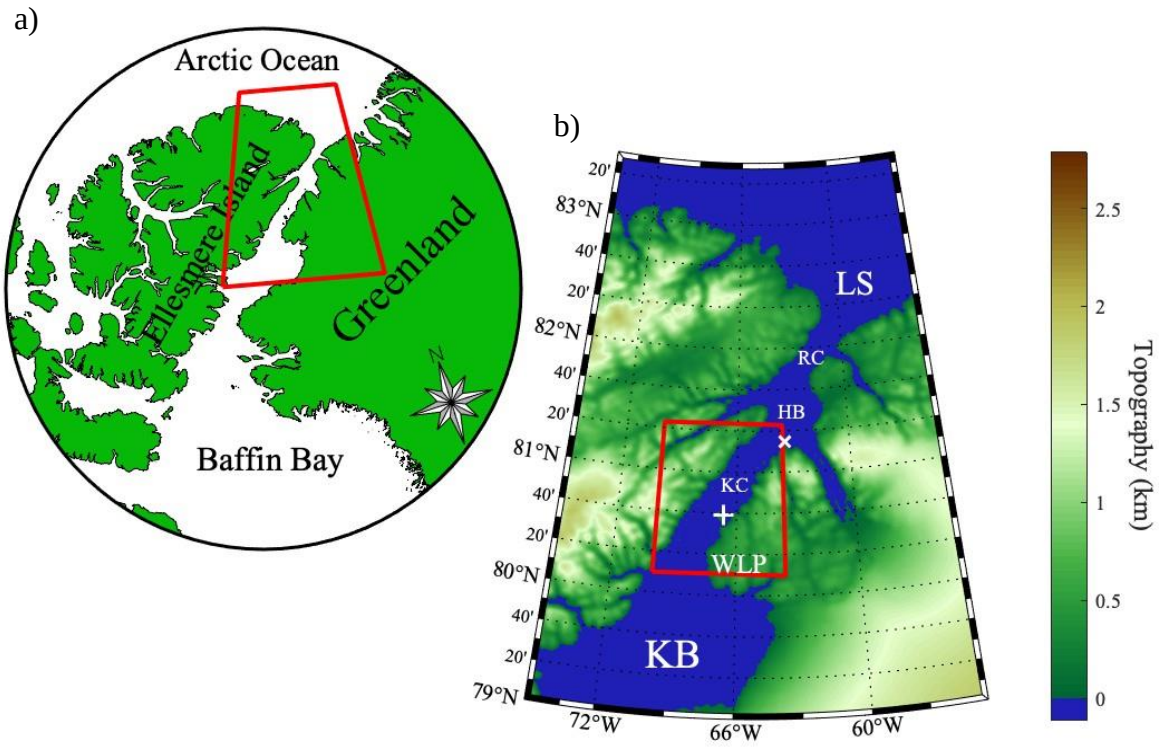


**Figure 1**. Geographical maps showing a) the location of Nares Strait and b) an enlarged view of the red-boxed region showing the topography around northern Nares Strait with the red polygon showing the specific domain in which sea ice and winds were analyzed. The labelled locations near and on the strait are: the Lincoln Sea (LS), Robeson Channel (RC), Hall Basin (HB), Kennedy Channel (KC), Washington Land Peninsula (WLP), Kane Basin (KB), Joe Island (x), and Franklin Island (+).

In this study we identify previously unknown transient polynyas that develop along Kennedy Channel that connects Hall Basin to Kane Basin (Fig. 1). These polynyas typically form downwind of Joe Island and Franklin Island that are situated along the channel. The winds along the channel tend to be enhanced as a result of its narrowness and the steep topography that borders it (Moore & Imrit, 2022). We suggest a mechanism by which these islands shield adjacent downwind areas from becoming ice-covered by southward sea ice flow as a result of strong wind-forced advection.

## 2 Materials and Methods

### 2.1 Datasets

In order to investigate this phenomenon, sea ice concentration along Nares Strait was retrieved with the ARTIST algorithm (Spreen et al., 2008) that makes use of data from the Advanced Microwave Scanning Radiometers (AMSR-E and AMSR2). The ARTIST dataset has

a spatial resolution of approximately 3.125 km and is available from June 2002 – August 2023, with a break between October 2011 and July 2012. In order to facilitate examination of atmospheric conditions surrounding Nares Strait, 10 m wind speed, wind direction, and mean sea-level pressure daily-averaged fields from the Copernicus Arctic Regional Reanalysis (CARRA) were used (Schyberg et al., 2020). The CARRA fields are available at a resolution of 2.5 km for the period from September 1990 – May 2023.

Imaging/mapping of the sea ice along Nares Strait was achieved using AMSR sea ice concentration data, MODIS (Moderate Resolution Imaging Spectroradiometer) infrared channels, as well as the AMSR's 89 GHz brightness temperature channels. Upwards vertically polarized emissions at 89 GHz made it possible to distinguish open water (greater brightness temperature) from sea ice (lower brightness temperature).

### 2.2 Choice of time period

Nares Strait's mobile sea ice season typically lasts from mid/late summer to mid/late winter (Vincent, 2019), with the rest of the year generally characterized by the presence of an ice arch along the strait that inhibits sea ice flow. October was found to be the ideal month for our analysis since it avoided the early sea ice transport season (September) during which sea ice concentration is low, while also avoiding the early onset of the ice arch season, which can begin as early as November. We did, however, redo our analysis for November and found similar results.

### 2.3 Peak Over Threshold Technique

To quantify sea ice concentration variability within Kennedy Channel, a spatial domain ranging from 80.16ºN to 81.38ºN latitude and 63.6ºW to 70ºW longitude was used (Fig. 1). The mean daily ice concentration in this region was calculated for all October days on record. We then employed a peak-over-threshold method by identifying the October dates with mean ice concentration values that exceeded the $90^{th}$ quantile value and the dates that lie below the $10^{th}$ quantile value, denoted as our high and low sea ice concentration events, respectively. In order not to bias our results, instances of double counting whereby we identified several consecutive days with a mean ice concentration that exceeded the thresholds were not considered. To account for this, whenever multiple days were found to lie beyond the lower or upper thresholds, only the

dates with the lowest or highest values, respectively, within a 3-day period were considered in the analysis. After identifying all dates that exceeded the thresholds, and accounting for the described double counting, a total of 30 high sea ice event dates and 33 low sea ice event dates were identified. We performed a repeat analysis by thresholding on extreme wind speed/direction events as well and obtained similar results.

Following identification of the October dates that fit into either category, sea ice concentration maps for northern Nares Strait for the high event dates and low event dates were composited. For comparison, the sea ice concentration maps for all available October days were also averaged to identify the climatological sea ice conditions. The 10 m wind vector fields and sea-level pressure maps from CARRA data for the high and low sea ice event dates were also composited and a climatological wind and sea-level pressure map was similarly obtained using data from all available October days.

Daily latitudinal profiles of sea ice concentration and wind speeds along Nares Strait were also constructed by determining median AMSR sea ice concentration and CARRA wind speeds parallel to the strait along lines of constant latitude. Composites of high and low sea ice event profiles were generated in order to facilitate a more quantitative treatment of our proposed island phenomenon. The climatological latitudinal profile from all available October days from 2002 – 2022 was again determined for comparison. Furthermore, using a Monte Carlo approach, the $1^{st}$ quantile and $99^{th}$ quantile of sea ice concentration and wind speed considering all October days and at each available latitude were determined in order to characterize the statistical significance of the high and low composites.

# 3 Results

## 3.1 Temporal Variability of Sea Ice

We calculated the mean daily sea ice concentration along Kennedy Channel during October 2002 – 2022 and constructed a time series for a typical month — October 2022 (Fig. 2). It is evident here that the sea ice concentration is quite variable with a mean of 64%, two events where the ice concentration drops below the 10$^{th}$ quantile value of 53%, as well as two events where the ice concentration rises above the 90$^{th}$ quantile value of 82%. Other Octobers during the period of interest had similar distributions.

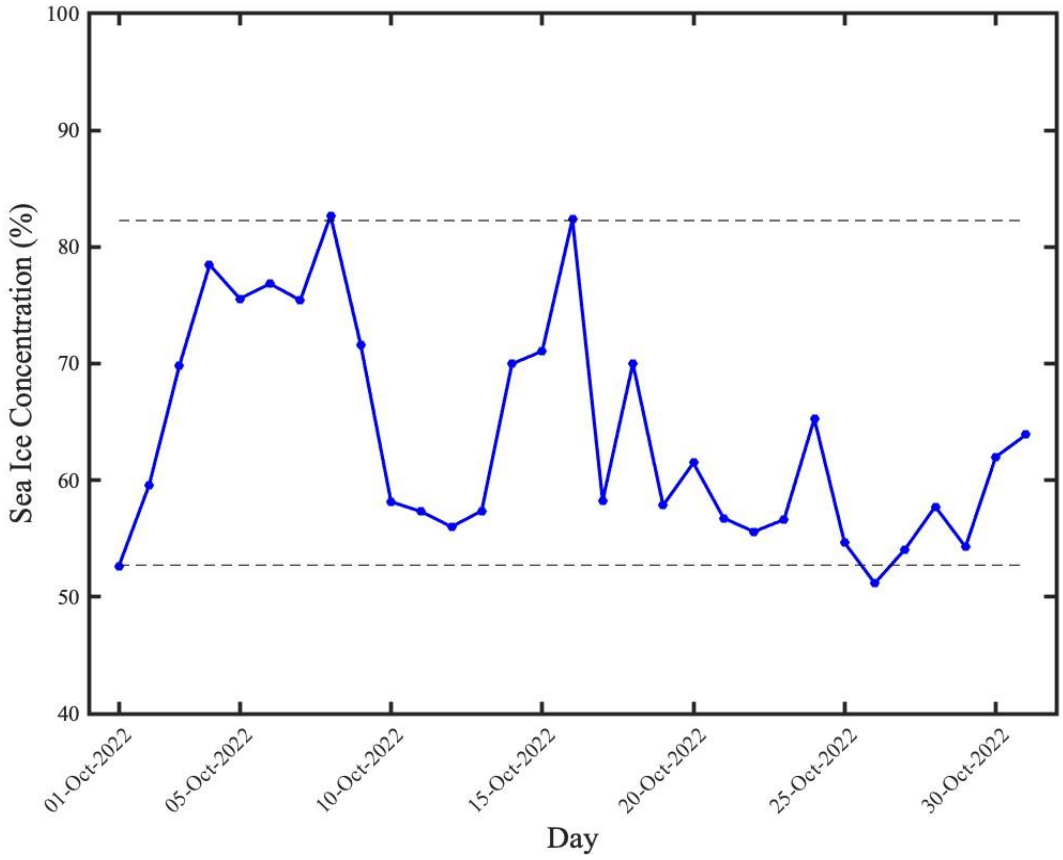


**Figure 2**. Time series of daily mean sea ice concentration (AMSR2) in Kennedy Channel during the month of October 2022. The horizontal dashed lines show the 90$^{th}$ quantile (upper line) and 10$^{th}$ quantile (lower line) values of mean daily sea ice concentration in this region during Octobers.

For the date that was identified with an average ice concentration lying below the lower threshold — Oct 26, 2022 — the reduced ice cover was mapped/imaged (Fig. 3). In each image

high quantities of sea ice can be observed throughout the strait and Kennedy Channel, with regions of open water and reduced ice cover southwards of Franklin Island and Joe Island.

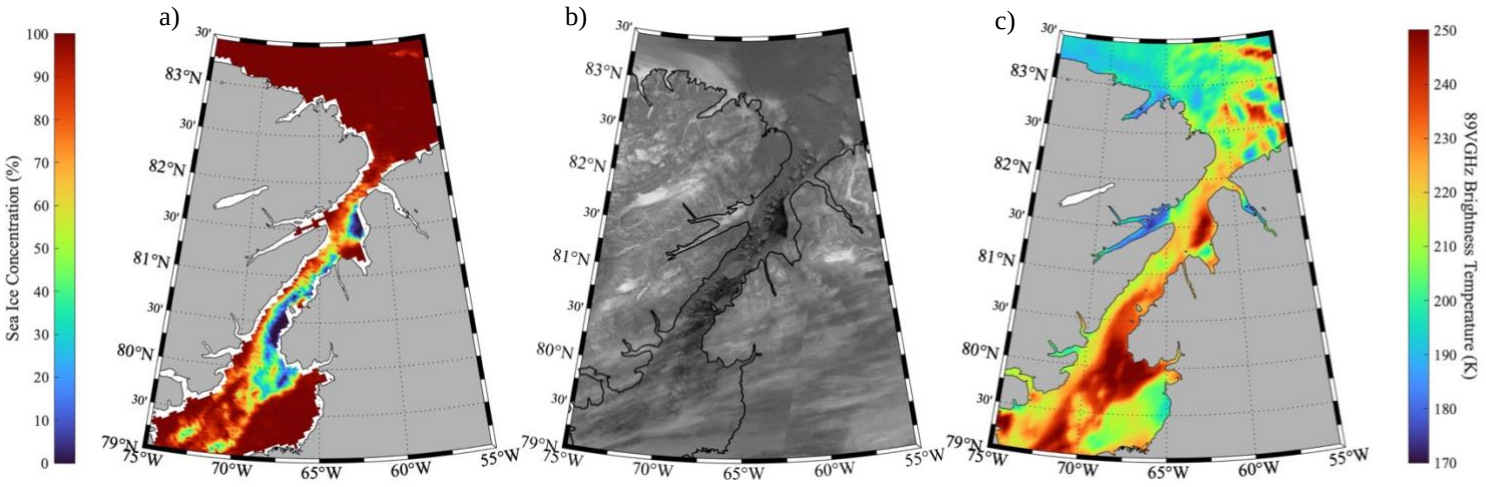


**Figure 3**. Kennedy Channel and Northern Nares Strait as viewed, using a) the mapping of AMSR2 sea ice concentration data, b) MODIS infrared imagery, and c) AMSR2 89GHz vertical polarization brightness temperature data, on October 26, 2022.

### 3.2 Spatial Variability of Sea Ice

The climatological sea ice distribution during October (Fig. 4a) indicates that the ice concentration is close to 100% over the Lincoln Sea and decreases as one moves southwards towards northern Kane Basin. Local minima occur south of Joe and Franklin Islands as well as over northern Kane Basin south of the Washington Land Peninsula (Fig. 1). The low event composite (Fig. 4b) has a quantitatively similar structure to the climatological case with significantly reduced sea ice concentrations in the same locations. The high event composite (Fig. 4c) shows nearly 100% ice cover from the Lincoln Sea down into Kane Basin, albeit with a similar noticeable minimum south of the Washington Land Peninsula.

The median sea ice concentration along the strait as a function of latitude provides a more quantitative view of sea ice variability in Nares Strait (Fig. 4d). Significant local minima for the low event case are observed directly downstream of the latitudes of Joe and Franklin Islands. Another local minimum is observed around 82°N. Interestingly, in the low composite, there was a sharp increase in ice presence immediately north of Franklin Island prior to the subsequent decrease to its south producing a sea ice dipole across the island. The climatological and high event cases show less variability in median ice concentration and are characterized by weaker local minima near the same latitudes as the low case. As expected, the lowest ice concentrations

occur for the low composite where, south of Joe Island, it approaches 45% and where, south of Franklin Island, it reaches between 20% – 30%. The extrema in this low event case were also found to lie outside of the range of extreme ice concentration variability of the climatological October case represented by the shading.

173

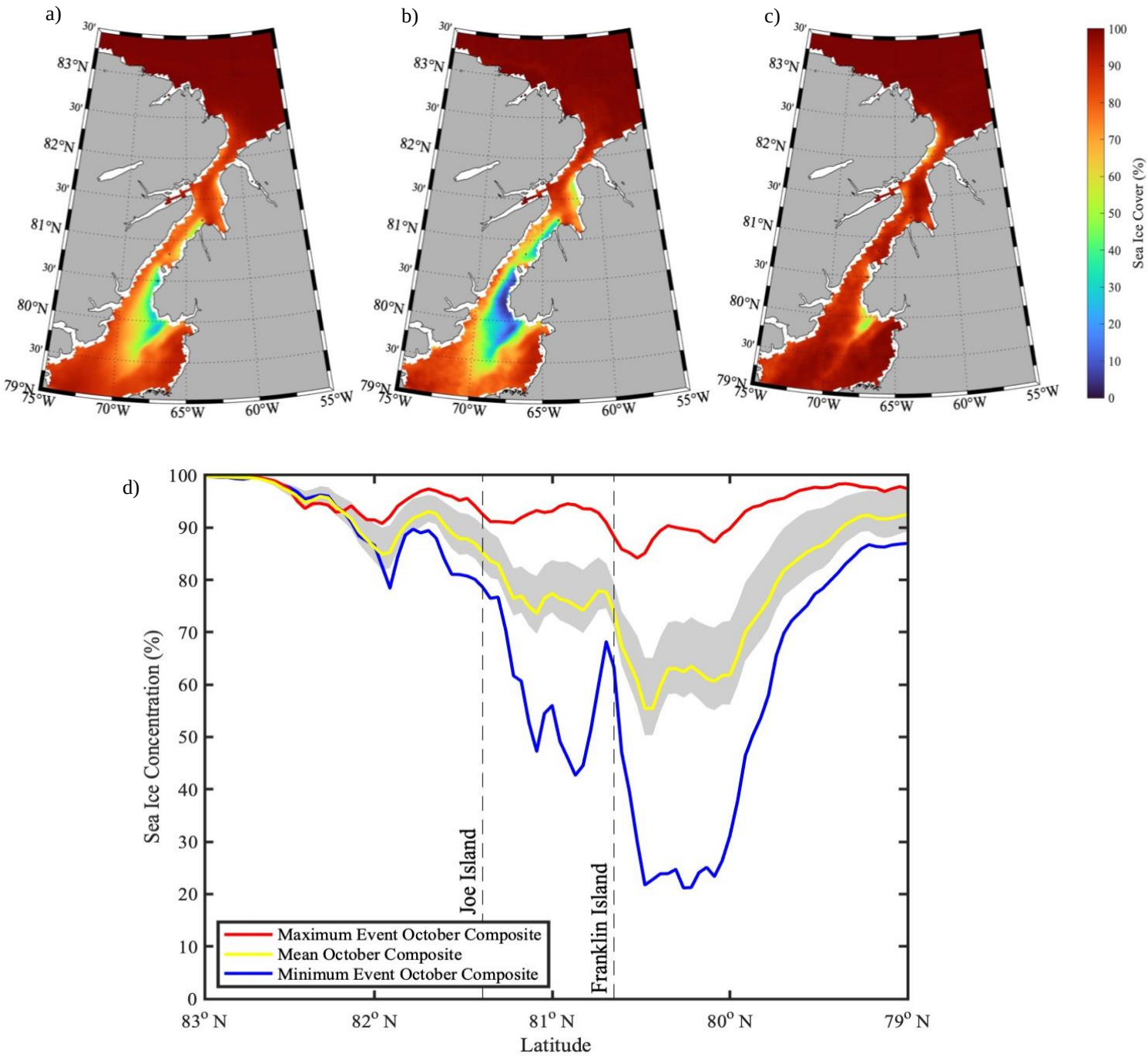


**Figure 4**. October spatial sea ice concentration composites for northern Nares Strait from 2002 – 2022. The three images correspond to the averaging of a) all October days, b) only low event October days, and c) only high event October days. d) shows the median sea ice concentration by latitude along Nares Strait for each of the three sets of days. The shading represents the 1st and 99th quantile variability of sea ice concentration about the climatological composite at each latitude. The labeled dashed lines identify the latitudinal locations of Joe Island and Franklin Island.

### 3.3 Spatial Variability of Wind and Mean Sea Level Pressure

Composites of 10 m winds, 10 m windspeed, and sea level pressure for the low and high events along with climatological conditions were produced in a similar fashion to the sea ice maps (Fig. 5). The climatological October case (Fig. 5a) shows relatively weak winds in the Lincoln Sea and Robeson Channel (Fig. 1), but stronger winds along Kennedy Channel and the northwestern part of Kane Basin. The low event regime (Fig. 5b) shows significantly greater wind speeds as compared to the climatological case, particularly within Kennedy Channel, and has the strongest winds of the three composites. Furthermore, in these two cases the winds generally lie parallel to the strait, with weaker winds in each of the composites occurring at sites where the wind vectors are nearly parallel with the isobars (i.e. the Lincoln Sea, Hall Basin (Fig. 1), and southern Kane Basin). Conversely, the strongest winds, within Kennedy Channel, occur where the wind vectors are nearly orthogonal on the isobars. The high event case (Fig. 5c) has very weak winds throughout the strait. Interestingly, a wind reversal was present in this composite which reached speeds of ~6 m/s in northern Robeson Channel and the Lincoln Sea.

The median wind speed parallel to the strait as a function of latitude (Fig. 5d) provides a quantitative examination of the wind variability along the strait. Several local minima in winds are located north of Joe Island in all three cases, as well as a broad minimum over Kennedy Channel from just below 81.5$^{o}$N to just above 80$^{o}$N in the low and climatological cases. Again, it is seen that the strongest wind speeds directed southwards along the strait occur for the low event case reaching speeds of up to 12 m/s. Furthermore, this wind profile lies almost consistently outside the extreme range of wind speed variability of the climatological October case represented by the shading.

196

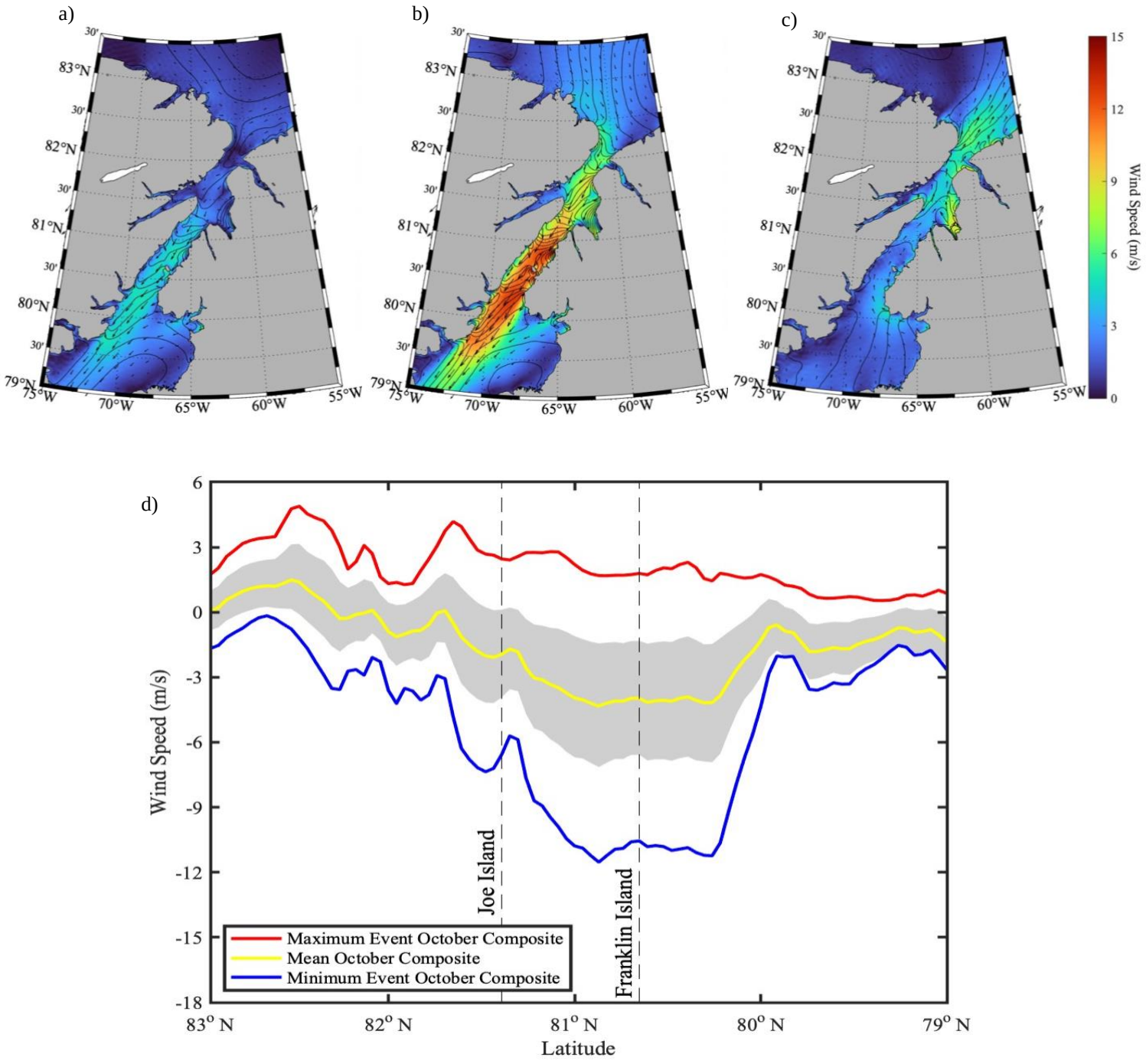


**Figure 5**. October spatial wind and pressure field composites for northern Nares Strait from 2002 – 2022. The maps show wind direction (vector field), wind speed (colourmap), and mean sea level pressure (isobar contours). The three composites were obtained from a) all October days, b) only low sea ice event days, and c) only high sea ice event days. d) shows the median wind speed parallel along the strait by latitude for each of the three sets of days. Positive values correspond to wind blowing up the strait while negative values correspond to wind blowing down the strait. The shading represents the 1st and 99th quantile variability of the wind speed about the climatological composite at each latitude. The labeled dashed lines identify the latitudinal locations of Joe Island and Franklin Island.

## 4 Discussion

In the low event case (Fig. 4b), it can be seen that the decrease in ice concentration within Kennedy Channel is the result of localized reductions at specific sites. The low ice concentrations south of the islands are believed to be caused by the advection of sea ice by winds into Kennedy Channel which, impinging upon the islands from the north, are diverted around them resulting in pockets of decreased concentration to form downwind. Since winds in this region generally blow from north to south (Moore, 2021), these polynyas tend to form off the southern faces of the islands.

These transient polynyas are believed to form analogously to wind-driven polynyas (Morales Maqueda et al., 2004) whereby coastal winds push sea ice away from land and expose open water. In Kennedy Channel, however, we propose that polynya production is caused by the southward wind-forced advection of ice around island obstacles, as opposed to the wind-forced removal of coastal ice.

Latitudinally, we find that the steepest local minima in ice concentration in the low event case occur south of the two islands, suggesting that it is indeed island effects that contribute to this behaviour (Fig. 4d). It is further seen that the minima latitudes in the low event October composite coincide with the minima in the climatological and high October composites at approximately 82$^{o}$N and south of Joe and Franklin Islands' latitudes. This quantitively demonstrates that this ice-shielding effect is noticeable even during climatological, and to some extent during high October sea ice conditions.

With respect to the wind and sea level pressure results (Fig. 5), the flow along Kennedy Channel can be seen to be ageostrophic which, as discussed by Moore and Imrit (2022), is a consequence of the narrowness of the Strait. In the low event regime (Fig. 5b), the pressure gradient along Kennedy Channel is larger and thus there are correspondingly greater wind speeds as compared to climatological (Fig. 5a) and high event regimes (Fig. 5c). These enhanced winds contribute to a strong ice advection effect around the islands and induce the formation of larger polynyas (Fig. 4b). These results suggest that the strength of southward winds through Kennedy Channel are directly correlated to the size and amount of ice reduction within these polynyas. In the upper extreme case (Fig. 5c) there are relatively weak winds in Kennedy Channel, and correspondingly no polynya can be observed in the ice concentration composite (Fig. 4c). The

noticeable sea ice reduction south of the Washington Land Peninsula (Fig. 4c) does, however, coincide with the ageostrophic flow of northwestern winds at this same site (Fig. 5c).

The wind fields in the low event composite and the climatological composite also reveal the presence of a meso-scale region of low pressure situated towards the eastern edge of Kane Basin bounded by the steep topography of the Washington Land peninsula to the north. This may be an example of a lee cyclone (Buzzi et al., 2020). The associated cyclonic circulation is more intense in the low event regime and would likely result in strong advection of sea ice away from the south side of Washington Land Peninsula, therefore contributing to the sea ice reduction observed here. It should be noted that a polynya had previously been identified in this region during June by Kirillov et al. (2022), yet its production was attributed to the melting of ice caused by the rising of warm subsurface water. We propose that a wind-driven sea ice advection effect may work in tandem with the upwelling of warm water to contribute to the formation of this polynya.

With respect to wind latitudinal profiles (Fig. 5d), the extreme winds in Kennedy channel agree with spatial wind observations in the low event case (Fig. 5b). Comparison of the ice and wind latitude profiles reveals that there is a correlated local minimum at approximately 82$^{o}$N shared among all composites. 82$^{o}$N marks a transitionary site whereby the geostrophic flow from the Lincoln Sea becomes ageostrophic in Robeson Channel (Fig. 5b). As the wind enters Nares Strait from the north, the narrow channel and steep topography funnel and accelerate the winds, thereby causing a spike in wind speed as observed in the wind speed profiles (Fig. 5d). Coincident sea ice flow carried by these winds into the strait is likely also sped up leading to a reduction and gap in ice presence as observed in the sea ice concentration profiles (Fig. 4d). This effect, albeit a small one, still produces a noticeable impact even on the high sea ice composite (Fig. 4d).

Downwind island effects have previously been shown to have far-reaching impacts on wind and sea temperature patterns in the Pacific Ocean (Xie et al., 2001). There is also evidence that the climatological easterly flow within the Chukchi Sea in the western Arctic Ocean results in a latent heat polynya downstream of Wrangel Island (Moore & Pickart, 2012). Here we identify previously unknown transient polynyas that form within the interior of Nares Strait due to such downstream island effects. The presence of these open water regions likely also lead to increased heat and moisture fluxes into the atmosphere from Kennedy Channel and potential

biological activity. Many Arctic species that overwinter in the Canadian Arctic Archipelago (Pole, 2016) may use these polynyas and may rely on them in a future where the NOW does not exist as it does today (Moore et al., 2023).

## Acknowledgments

## Open Research

AMSR-E and AMSR2 (Advanced Microwave Scanning Radiometer) data (Spreen et al., 2008) are available at https://seaice.uni-bremen.de/sea-ice-concentration/amsre-amsr2/. AMSR2 brightness temperature data (Meier et al., 2018) is available at https://nsidc.org/data/au_si6/versions/1#anchor-0. The CARRA (Copernicus Arctic Regional Reanalysis) data (Schyberg et al., 2020) areavailable at https://cds.climate.copernicus.eu/cdsapp#!/dataset/reanalysis-carra-single-levels?tab=overview.

## References


Arrigo, K. R. (2007). Chapter 7 Physical Control of Primary Productivity in Arctic and Antarctic Polynyas. In W. O. Smith & D. G. Barber (Eds.), *Polynyas: Windows to the World* (Vol. 74, pp. 223–238). Elsevier. https://doi.org/https://doi.org/10.1016/S0422-9894(06)74007-7

Barber, D. G., Hanesiak, J. M., Chan, W., & Piwowar, J. (2001). Sea-ice and meteorological conditions in Northern Baffin Bay and the North Water polynya between 1979 and 1996. *Atmosphere - Ocean*, *39*(3), 343–359. https://doi.org/10.1080/07055900.2001.9649685

Barber, D. G., & Massom, R. A. (2007). Chapter 1 The Role of Sea Ice in Arctic and Antarctic Polynyas. In W. O. Smith & D. G. Barber (Eds.), *Polynyas: Windows to the World* (Vol. 74, pp. 1–54). Elsevier. https://doi.org/https://doi.org/10.1016/S0422-9894(06)74001-6

Buzzi, A., Davolio, S., & Fantini, M. (2020). Cyclogenesis in the lee of the Alps: a review of theories. *Bulletin of Atmospheric Science and Technology*, *1*(3), 433–457. https://doi.org/10.1007/s42865-020-00021-6

Finley, K. J., & Renaud, W. E. (1980). Marine Mammals Inhabiting the Baffin Bay North Water in Winter. *Arctic*, *33*(4), 724–738.

Heide-Jørgensen, M. P., Burt, L. M., Hansen, R. G., Nielsen, N. H., Rasmussen, M., Fossette, S., & Stern, H. (2013). The significance of the north water polynya to arctic top predators. *Ambio*, *42*(5), 596–610. https://doi.org/10.1007/s13280-012-0357-3

Heide-Jørgensen, M. P., Sinding, M.-H. S., Nielsen, N. H., Rosing-Asvid, A., & Hansen, R. G. (2016). Large numbers of marine mammals winter in the North Water polynya. *Polar Biology*, *39*(9), 1605–1614. https://doi.org/10.1007/s00300-015-1885-7

Howell, S. E. L., Babb, D. G., Landy, J. C., Moore, G. W. K., Montpetit, B., & Brady, M. (2023). A Comparison of Arctic Ocean Sea Ice Export Between Nares Strait and the Canadian Arctic Archipelago. *Journal of Geophysical Research: Oceans*, *128*(4). https://doi.org/10.1029/2023JC019687

Ingram, R. G., Bâcle, J., Barber, D. G., Gratton, Y., & Melling, H. (2002). An overview of physical processes in the North Water. *Deep-Sea Research Part II: Topical Studies in Oceanography*, *49*(22–23), 4893–4906. https://doi.org/10.1016/S0967-0645(02)00169-8

Kirillov, S., Dmitrenko, I., Babb, D. G., Ehn, J. K., Koldunov, N., Rysgaard, S., Jensen, D., & Barber, D. G. (2022). The role of oceanic heat flux in reducing thermodynamic ice growth

in Nares Strait and promoting earlier collapse of the ice bridge. *Ocean Science*, *18*(5), 1535–1557. https://doi.org/10.5194/os-18-1535-2022

Kottmeier, Ch., & Engelbart, D. (1992). Generation and atmospheric heat exchange of coastal polynyas in the Weddell Sea. *Boundary-Layer Meteorology*, *60*(3), 207–234. https://doi.org/10.1007/BF00119376

Marchese, C., Albouy, C., Tremblay, J. É., Dumont, D., D'Ortenzio, F., Vissault, S., & Bélanger, S. (2017). Changes in phytoplankton bloom phenology over the North Water (NOW) polynya: a response to changing environmental conditions. *Polar Biology*, *40*(9), 1721–1737. https://doi.org/10.1007/s00300-017-2095-2

Meier, N., W., Comiso, J. C., & Markus, T. (2018). *AMSR-E/AMSR2 Unified L3 Daily 6.25 km Polar Gridded 89 GHz Brightness Temperatures, Version 1* [Dataset]. NASA National Snow and Ice Data Center Distributed Active Archive Center.

Møller, E. F., Johansen, K. L., Agersted, M. D., Rigét, F., Clausen, D. S., Larsen, J., Lyngs, P., Middelbo, A., & Mosbech, A. (2018). Zooplankton phenology may explain the North Water polynya's importance as a breeding area for little auks. *Marine Ecology Progress Series*, *605*, 207–223.

Moore, G. W. K. (2021). Impact of model resolution on the representation of the wind field along Nares Strait. *Scientific Reports*, *11*(1), 1–14. https://doi.org/10.1038/s41598-021-92813-9

Moore, G. W. K., Howell, S. E. L., & Brady, M. (2023). Evolving relationship of Nares Strait ice arches on sea ice along the Strait and the North Water, the Arctic's most productive polynya. *Scientific Reports*, *13*(1), 1–16. https://doi.org/10.1038/s41598-023-36179-0

Moore, G. W. K., & Imrit, A. A. (2022). Impact of Resolution on the Representation of the Mean and Extreme Winds Along Nares Strait. *Journal of Geophysical Research: Atmospheres*, *127*(19), 1–17. https://doi.org/10.1029/2022JD037443

Moore, G. W. K., & Pickart, R. S. (2012). The Wrangel Island Polynya in early summer: Trends and relationships to other polynyas and the Beaufort Sea High. *Geophysical Research Letters*, *39*(5), 1–5. https://doi.org/10.1029/2011GL050691

Morales Maqueda, M. A., Willmott, A. J., & Biggs, N. R. T. (2004). Polynya dynamics: A review of observations and modeling. *Reviews of Geophysics*, *42*(1). https://doi.org/10.1029/2002RG000116

Pole, N. (2016). *Canadian High Arctic-North Greenland LME*. 1–9.

Ribeiro, S., Limoges, A., Massé, G., Johansen, K. L., Colgan, W., Weckström, K., Jackson, R., Georgiadis, E., Mikkelsen, N., Kuijpers, A., Olsen, J., Olsen, S. M., Nissen, M., Andersen, T. J., Strunk, A., Wetterich, S., Syväranta, J., Henderson, A. C. G., Mackay, H., … Davidson, T. A. (2021). Vulnerability of the North Water ecosystem to climate change. *Nature Communications*, *12*(1). https://doi.org/10.1038/s41467-021-24742-0

Richard, P. R., Orr, J. R., Dietz, R., & Dueck, L. (1998). Sightings of Belugas and Other Marine Mammals in the North Water, Late March 1993. *Arctic*, *51*(1), 1–4.

Schyberg, H., Yang, X., Køltzow, M. A. Ø., Amstrup, B., Bakketun, Å., Bazile, E., Bojarova, J., Box, J. E., Dahlgren, P., Hagelin, S., Homleid, M., Horányi, A., Høyer, J., Johansson, Å., Killie, M. A., Körnich, H., Le Moigne, P., Lindskog, M., Manninen, T., … Wang, Z. Q. (2020). *Arctic regional reanalysis on single levels from 1991 to present*. Copernicus Climate Change Service (C3S) Climate Data Store (CDS). https://doi.org/10.24381/cds.713858f6

Smedsrud, L. H., Halvorsen, M. H., Stroeve, J. C., Zhang, R., & Kloster, K. (2017). Fram Strait sea ice export variability and September Arctic\hack{\newline} sea ice extent over the last 80 years. *The Cryosphere*, *11*(1), 65–79. https://doi.org/10.5194/tc-11-65-2017

Smith, S. D., Muench, R. D., & Pease, C. H. (1990). Polynyas and leads: An overview of physical processes and environment. *Journal of Geophysical Research: Oceans*, *95*(C6), 9461–9479. https://doi.org/https://doi.org/10.1029/JC095iC06p09461

Spreen, G., Kaleschke, L., & Heygster, G. (2008). Sea ice remote sensing using AMSR-E 89-GHz channels. *Journal of Geophysical Research: Oceans*, *113*(2), 1–14. https://doi.org/10.1029/2005JC003384

Steffen, K. (1985). Warm water cells in the North Water, Northern Baffin Bay during winter. *Journal of Geophysical Research: Oceans*, *90*(C5), 9129–9136. https://doi.org/10.1029/jc090ic05p09129

Tremblay, J.-E., & Smith, W. O. (2007). Chapter 8 Primary Production and Nutrient Dynamics in Polynyas. In W. O. Smith & D. G. Barber (Eds.), *Polynyas: Windows to the World* (Vol. 74, pp. 239–269). Elsevier. https://doi.org/https://doi.org/10.1016/S0422-9894(06)74008-9

Vincent, R. F. (2019). A Study of the North Water Polynya Ice Arch using Four Decades of Satellite Data. *Scientific Reports*, *9*(1), 20278. https://doi.org/10.1038/s41598-019-56780-6

Weingartner, T. J., Cavalieri, D. J., Aagaard, K., & Sasaki, Y. (1998). Circulation, dense water formation, and outflow on the northeast Chukchi Shelf. *Journal of Geophysical Research: Oceans*, *103*(C4), 7647–7661. https://doi.org/https://doi.org/10.1029/98JC00374

Xie, S. P., Liu, W. T., Liu, Q., & Nonaka, M. (2001). Far-Reaching effects of the Hawaiian islands on the Pacific Ocean-Atmosphere system. *Science*, *292*(5524), 2057–2060. https://doi.org/10.1126/science.1059781